ELSEVIER

Journal of Power Sources 104 (2002) 272–280

JOURNAL OF POWER SOURCES

www.elsevier.com/locate/jpowsour

X-ray diffractometric study of in situ oxidation of Ni in Li/K and Li/Na carbonate eutectic

T. Kudo[a,*], Y. Hisamitsu[b], K. Kihara[b], M. Mohamedi[b], I. Uchida[c]

[a]*Research and Development Center, Tohoku Electric Power Co., Inc., 7-2-1 Nakayama, Aoba-Ward, Sendai-City, Miyagi 981-0952, Japan*
[b]*Department of Applied Chemistry, Graduate School of Engineering, Tohoku University, 07 Aramaki-Aoba, Aoba-Ward, Sendai-City, Miyagi 980-8579, Japan*
[c]*New Industry Creation Hatchery Center, Tohoku University, 04 Aramaki-Aoba, Aoba-Ward, Sendai-City, Miyagi 980-8579, Japan*

Received 2 July 2001; received in revised form 13 September 2001; accepted 25 September 2001

Abstract

The formation of NiO, particularly the lithiation process, in molten carbonate at 923 K under oxidizing condition has been investigated by open circuit potential (OCP), AC impedance, and X-ray diffraction (XRD) measurements. Thin film electrodes of Ni were exposed to the Li/K and Li/Na carbonate eutectic and subjected to in situ oxidation. Quantification of lithium in the lithiated NiO with XRD revealed that the lithiation reaction continues even after the electrode potential reached the oxygen electrode potential. Lithium content, x in $Li_xNi_{1-x}O$, of the sample immersed in molten carbonate reached 0.041 and 0.033 in Li/K and Li/Na melt, respectively after 200 h of immersion. Difference observed in OCP decay and electrode impedance at 1 kHz for Ni oxidation in the Li/K and Li/Na carbonate has been also interpreted based on XRD data.

Keywords: MCFC; NiO; In situ oxidation; Li content; X-ray diffraction; Lattice parameter

1. Introduction

Molten carbonate fuel cell (MCFC) is still under consideration [1,2] as one of the most promising efficient and environmentally friendly power systems. However, the life span of the MCFC remains insufficient for commercial use. It is commonly recognized that the internal short-circuiting caused by the dissolution of NiO cathode is the most serious issue to tackle for long-term operation of the MCFC. Thus, alternative cathode materials are being sought [3–12] to extend the MCFC's lifetime up to 40,000 h that is the requirement for commercialization. To develop countermeasures for NiO dissolution, it is important to understand the mechanism of in situ NiO formation. Nishina et al. investigated the in situ formation of NiO in molten Li/K carbonate using open circuit potential (OCP) measurements and X-ray photoelectron spectroscopy (XPS) [13]. Three potential plateaus were observed which were attributed to (i) oxidation of Ni to NiO, (ii) oxidation of Ni(II) to Ni(III) in the NiO lattice accompanied by lithiation, and (iii) oxygen electrode reaction. That is

$$Ni + CO_3^{2-} \rightarrow NiO + CO_2 + 2e^-$$

$$Ni_{Ni}^{2+} + O^{2-} \rightarrow []''_{Ni} + Ni_{Ni}^{3+} + O_O^{2-} + e^-$$

$$[]''_{Ni} + Li^+ \rightarrow [Li]'_{Ni}$$

$[]''_{Ni}$ and $[Li]'_{Ni}$ denote a Ni vacancy and a Li^+ doped into Ni vacancy in the NiO lattice, respectively.

Tomczyk et al. [14] reconsidered the foregoing mechanism and proposed the formation of an unstable intermediate, namely, $NiCO_3$.

$$Ni + CO_3^{2-} \rightarrow NiCO_3 + 2e^-$$

$$NiCO_3 \rightarrow NiO + CO_2$$

Yazici and Selman [15] by means of an optical microscope observed the surface of Ni being oxidized in situ. According to the authors, a porous structure of in situ NiO is formed at the third potential plateau of the OCP profile. In our previous work [16], the surface morphology of the lithiated NiO at Stage III was observed with an atomic force microscopy and we reached to a similar conclusion as Yazici and Selman [15]. According to these observations [15,16], one can assume that the drastic change in the surface morphology of NiO at Stage III of OCP is related to the insertion of Li^+ into NiO. This hypothesis partially contradicts the mechanism proposed by Nishina et al. [13] claiming that the lithiation process ends at Stage II. If the Li content in $Li_xNi_{1-x}O$ compound could be quantified during in situ oxidation of Ni, one can obtain an evidence to judge when the lithiation occurs predominantly. Several authors have attempted to estimate the Li content in $Li_xNi_{1-x}O$ [17–19].

* Corresponding author. Fax: +81-22-278-0506.
E-mail address: tkudo@rdc.tohoku-epco.co.jp (T. Kudo).

0378-7753/02/$ – see front matter
PII: S0378-7753(01)00962-4

For example, Belhomme et al. [18] measured lithium concentration and its depth profile in the NiO with a nuclear microprobe. However, these studies were carried out ex situ, i.e. after the lithiation was completed. In this paper, the lithium content in NiO was estimated based on the variation of its cubic lattice parameter during in situ oxidation.

2. Experimental

Procedure of melt purification, gas handling, temperature control, and cell assembly have been described elsewhere [13,20–22]. The working electrode consisted of a thin layer (0.75 μm thickness) of Ni plated onto both sides of a gold flag substrate (0.39 cm^2) denoted henceforth as Ni/Au, which was fully immersed in the melt. The Watt's nickel bath was used for plating. All electrochemical measurements were conducted in $(Li_{0.62}K_{0.38})_2CO_3$ and $(Li_{0.53}Na_{0.47})_2CO_3$ eutectics (denoted henceforth as Li/K and Li/Na, respectively) at 923 K. The OCP and the AC impedance at 1 kHz were recorded simultaneously during the oxidation process with a Solartron 1286 potentiostat in combination with a Solartron 1260 frequency response analyzer. Detailed procedure of the OCP and AC impedance measurement is reported elsewhere [13]. Electrochemical potential was referred to the standard (O_2:CO_2 = 0.33:0.67 atm)|Au gas reference electrode denoted henceforth as SOE. The surrounding gas was O_2:CO_2 = 0.9 atm:0.1 atm, which was fed from a gas cylinder of premixed O_2:CO_2 = 9 : 1 (Sumitomo Seika Chemicals).

A fresh Ni/Au and a pre-oxidized Ni/Au were tested in Li/K eutectic. The pre-oxidized samples of Ni/Au were obtained by heating the Ni/Au at 923 K in the air for 12 h. Prior and after exposure to the melt, all samples were characterized ex situ with a Rigaku RINT-2500 X-ray diffractometer (XRD) equipped with a thin film attachment using Cu Kα radiation. Two θ scan mode with an incident angle of two degrees was employed for thin film XRD measurements. X-ray power was set at 40 kV, 200 mA. Scan step and integration time per step was set at 0.002 ° and 6 s, respectively, for profile measurements. For the lattice parameter refinements, the integration time was adjusted to achieve 1000 counts of integration intensity equally for every peak of interest. This technique enables to ensure sufficient intensity for high-angle peaks. Credibility of refined lattice parameter was estimated according to the standard deviations (σ), which were obtained with Eq. (1). Variable "a" is the lattice parameter, which is available from each peak position independently in case of cubic setting. Suffix "obs" and "fit" denotes "observed" and "fitted" values, respectively. Peaks employed to refine lattice parameter were NiO(1 1 1), (2 0 0), (2 2 0), (3 1 1), (2 2 2), (4 0 0), and (3 3 1).

$$\sigma = \sqrt{\frac{\sum_{n=1}^{7}(a_{\mathrm{obs}_n} - a_{\mathrm{fit}})^2}{7}} \quad (1)$$

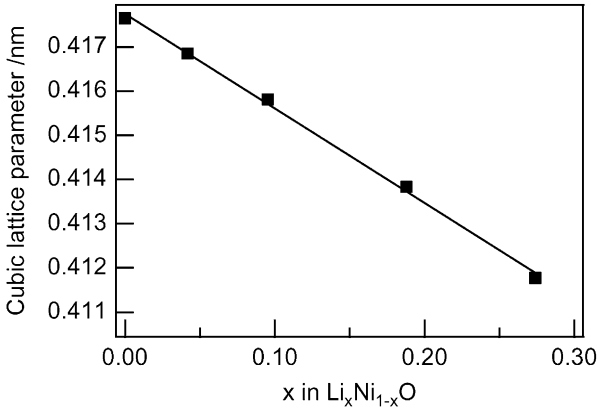

Fig. 1. Correlation between x in $Li_xNi_{1-x}O$ and its lattice parameter in cubic setting. Data were cited from [23].

Within 200 h of exposure in the carbonate melt, samples were withdrawn from the melt periodically, rinsed with distilled water, dried at 120 °C in air, and subjected to XRD. Lithium content in the lithiated NiO ($Li_xNi_{1-x}O$) was determined based on the variation in cubic lattice parameter of $Li_xNi_{1-x}O$ with x as reported by Sato et al. [23]. Fig. 1 shows the correlation between x in $Li_xNi_{1-x}O$ and cubic lattice parameter. When refining the lattice parameter, deviations of peak position from the intrinsic one were compensated against the peaks of gold substrate, which was exploited as an internal standard material. We adopted 0.40786 nm as the cubic lattice parameter of Au (JCPDS 4-784).

3. Results

3.1. In situ oxidation of Ni in Li/K eutectic

The OCP response of a fully immersed Ni/Au electrode is shown in Fig. 2. Three distinct stages can be observed for the in situ oxidation of Ni in the Li/K carbonate melt. In Stage I, the electrode potential initially of −0.74 V versus SOE gradually shifted to reach a potential around −0.34 V versus SOE (Stage II), where it retained for 3.5 h. Finally, the electrode potential approached the oxygen reduction equilibrium potential (Stage III).

Fig. 3 shows XRD patterns of Ni/Au withdrawn from the melt at various time points after immersion. As can be seen from Fig. 3, the XRD profile varied with the progress of in situ oxidation. Observed Bragg peak positions agree well with those reported in reference pattern, Ni (JCPDS 4-850), NiO (JCPDS 47-1049), and Au (JCPDS 4-784). Peaks marked by filled squares in Fig. 3 could not be attributed to specific phases. However, we found that $NiCO_3$ (JCPDS 12-771) is the most plausible phase among possible compounds, which supports the prediction of Tomczyk et al. [14].

Variation in the cubic lattice parameter of the oxidized product with time is shown in Fig. 4 altogether with the OCP

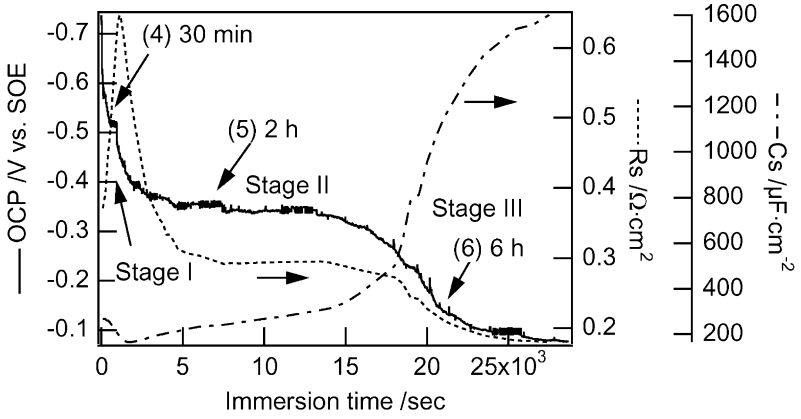

Fig. 2. Change in OCP, resistance (R_S) and capacitance (C_S) of C–R series circuit with time of Ni thin film (0.75 μm thickness) on Au foil electrode in $(Li_{0.62}K_{0.38})_2CO_3$ at 923 K under $P_{O_2} : P_{CO_2} = 0.9 : 0.1$ atm.

response. Bars indicate standard deviations (σ) obtained using Eq. (1). Numbers between brackets correspond to the number of XRD profile (Fig. 3). The samples, withdrawn within 30 min of exposure, showed experimental error larger than the others because of hindrance of impurity phases other than NiO. According to the previous work [23,24], the cubic lattice parameter of $Li_xNi_{1-x}O$ decreases linearly with the increase of x when x is smaller than 0.31 as shown in

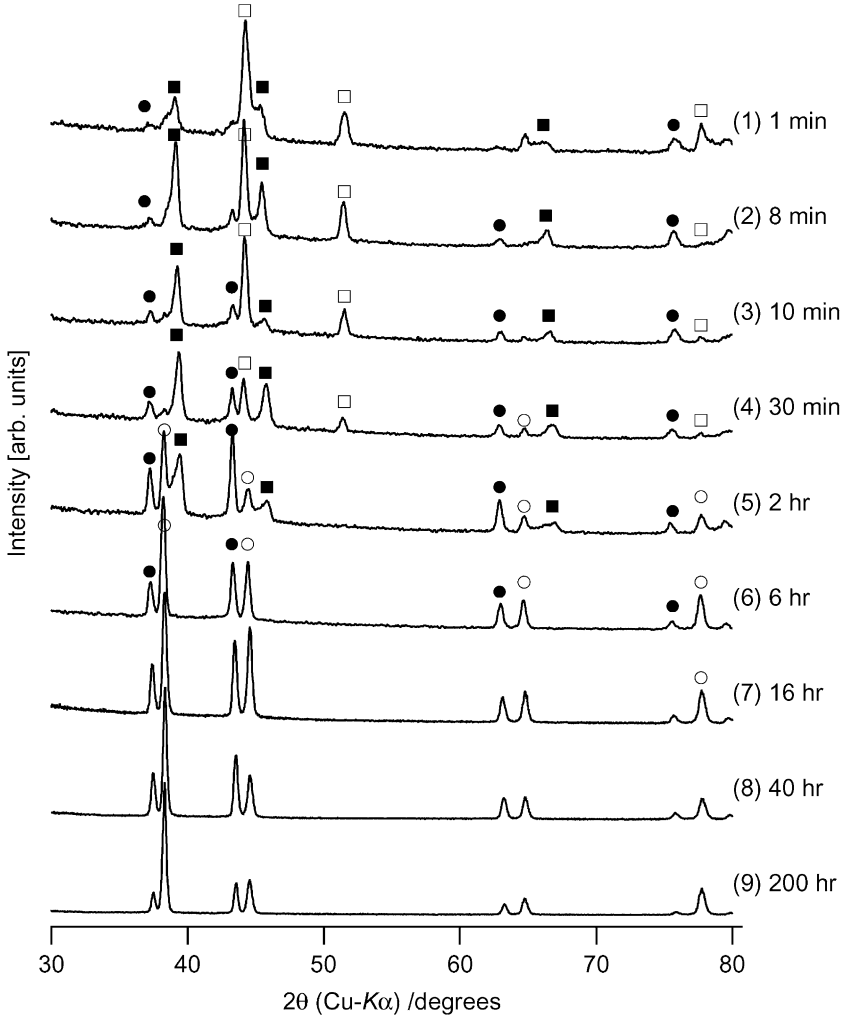

Fig. 3. XRD patterns of Ni/Au samples withdrawn at various time of exposure from $(Li_{0.62}K_{0.38})_2CO_3$ melt at 923 K under $P_{O_2} : P_{CO_2} = 0.9 : 0.1$ atm. (○): Au, (□): Ni, (●): NiO, (■): $NiCO_3$.

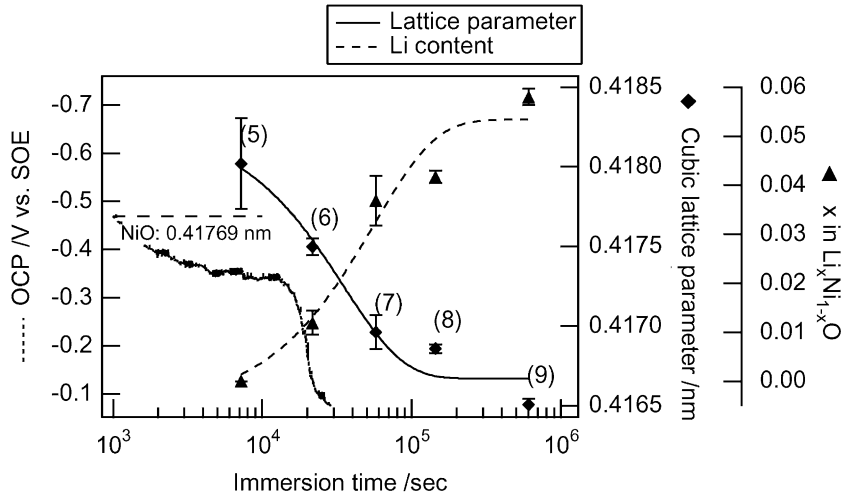

Fig. 4. Change in cubic lattice parameter and Li content of NiO with time. Numbers in the parenthesis correspond to Fig. 3.

Fig. 1. According to Fig. 1, a correlation between the lattice parameter and the lithium content was found as

$$x = 19.479 - 46.628a \quad (2)$$

where "a" and "x" represent the cubic lattice parameter and lithium content, respectively. From Eq. (2), one obtains $x = 0.003$ for a lattice parameter of NiO (without Li) of $a = 0.41769$. The value of 0.003 is smaller than a series of standard deviations in this paper. Thus, Eq. (2) is accurate enough to estimate the lithium content in our measurements. By means of Eq. (2), the variation in x with immersion time is gathered in Fig. 4. The lattice parameter of sample no. 5 (0.4180(3) nm) agrees with the lattice parameter of NiO (0.41769 nm, JCPDS 47-1049) within the experimental error. Thus, the lithium content of the sample no. 5 can be regarded as zero. The correlation between the lithium content and OCP suggests that the lithiation reaction continues even after the OCP has reached the oxygen electrode potential. After 200 h of immersion, the lithium content x reached 0.058(2). This value is larger than the recent value of 0.04 reported by Selman and Maru [25]. The peak intensity of NiO at 200 h (sample no. 9 in Fig. 3) was relatively weak in comparison to that of Au substrate. It suggests that NiO was partially dissolved into the melt during 200 h of immersion. Thus, the lattice parameter of the sample no. 9 is less credible than those of the others. Judging from the lattice parameter of the sample no. 8 (40 h of immersion), the lithium content x was 0.041(1), which agrees well with the reference value [25].

Next, a comparative study was performed with a pre-oxidized Ni/Au. Fig. 5 shows the variation of the lattice parameter with Eq. (2) versus immersion time and lithium content. Prior to immersion, the lattice parameter was 0.41770(3) nm, which agrees well with the reported value

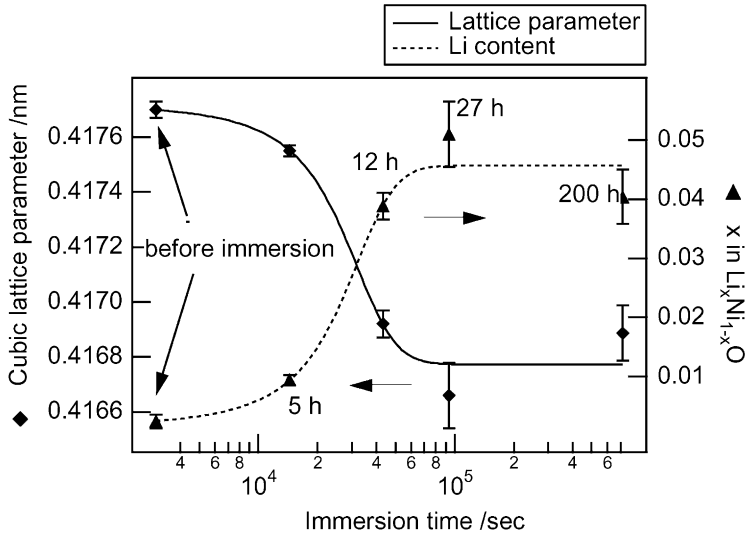

Fig. 5. Change in cubic lattice parameter and Li content of pre-oxidized NiO with time in $(Li_{0.62}K_{0.38})_2CO_3$ melt at 923 K under $P_{O_2} : P_{CO_2} = 0.9 : 0.1$ atm.

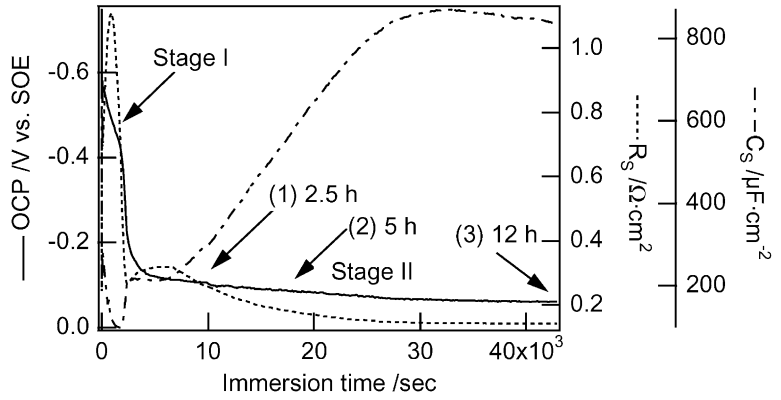

Fig. 6. Change in OCP and resistance (R_S), capacitance (C_S) of C–R series circuit with time on Ni thin film (0.75 μm thickness) on Au foil electrode in $(Li_{0.53}Na_{0.47})_2CO_3$ at 923 K under $P_{O_2} : P_{CO_2} = 0.9 : 0.1$ atm.

of NiO without Li (0.41769 nm, JCPDS 47-1049). After 200 h, the lattice parameter reached 0.41688(2) nm, which corresponds to a lithium content of 0.040(5). The difference among the values obtained at 12, 27, and 200 h of immersion is insignificant because of their standard deviations. Thus, the intrinsic lithium content of the pre-oxidized Ni/Au after lithiation should be estimated to be within 0.04–0.05 range, which also agrees with the reference value [25].

3.2. *In situ oxidation of Ni in Li/Na eutectic*

Fig. 6 shows time-evolution of the OCP and electrode impedance at 1 kHz during in situ oxidation of Ni/Au in Li/Na melt. It exhibits two stages denoted as Stages I and II in Fig. 6. Electrode potential at the Stage I can be attributed to Ni(II)/Ni(III) system according to thermodynamic data [26]. Fig. 7 shows a magnified view of Stage I in Fig. 6. The shape of the OCP curve is similar to the one reported by Tomczyk and Mosialek [27] for Li/Na melt over a period of 2.8 h after immersion. In previous works [8,13,27], only the Stage I was considered as a major issue of in situ formation of NiO. However, sluggish anodic shift of OCP and distinct change in electrode impedance (R_S and C_S) is observed at the Stage II in Fig. 6. In particular, steep increase of C_S suggests some kind of change in the crystallographic phase or surface morphology of the sample. Fig. 8 shows XRD profiles of Ni/Au withdrawn from the Li/Na melt at various time of exposure. The Bragg peaks were almost identical to those obtained in Li/K melt. Samples withdrawn at 2.5 and 5 h immersion contained $NiCO_3$. The 12 h immersed sample also contained small amount of $NiCO_3$ and unknown impurities. Magnified view of XRD for 12 h immersed sample is shown in Fig. 9. Reflection of Cu $K\alpha_2$ was subtracted to distinguish overlapped peaks. One can recognize extra peaks superimposed on the Au(1 1 1), (2 0 0), and (3 1 1) peaks. Peaks of $NiCO_3$ diminished in intensity with time and vanished by 17 h. Fig. 10 shows SEM images of the sample at various time of exposure. In the beginning, the surface exhibits fine particles at 2.5 and 5 h. Subsequently, octahedral particles appeared on the surface at 12 h, which are thought to be particles of NiO single crystal. Finally, octahedral particles grew up to cover the surface (Fig. 10 (4)). According to XRD profiles and SEM images, nickel carbonate decomposes to NiO and crystallinity of NiO increases at the Stage II in Fig. 6. This process enlarges the relative surface area of the sample, which results in steep increase of C_S. Steep increase of C_S at Stage III in Li/K melt (Fig. 2) would be also a result of decomposition of $NiCO_3$. This is

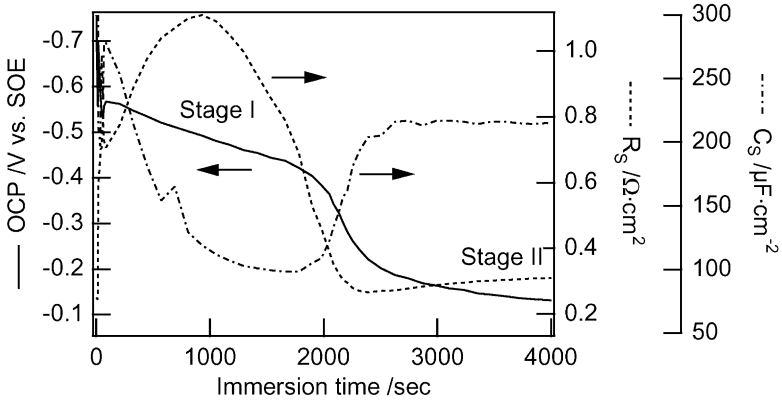

Fig. 7. Magnified view of Stage I in Fig. 6.

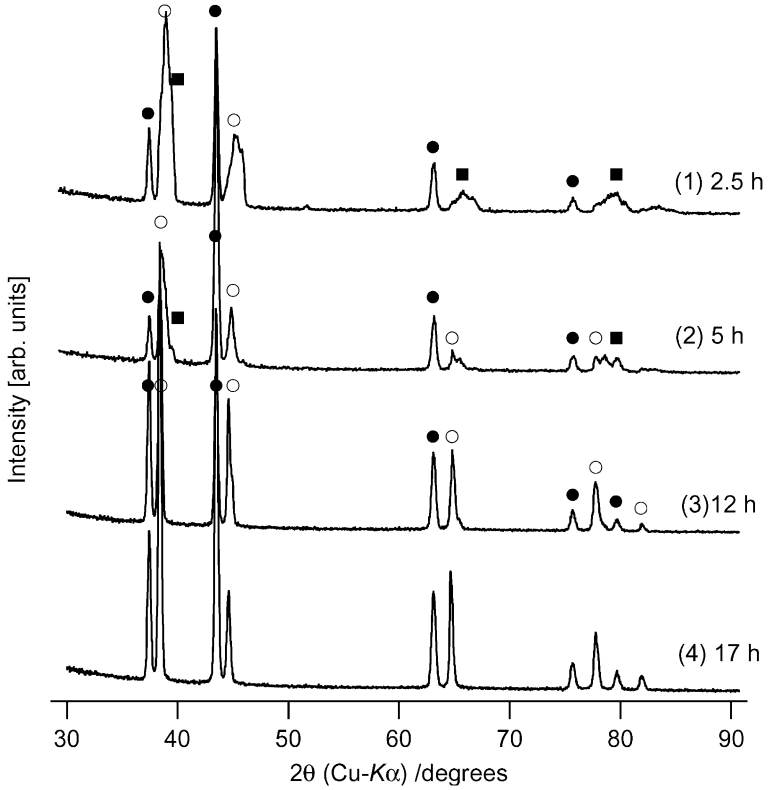

Fig. 8. XRD patterns of Ni/Au samples withdrawn at various time of exposure from $(Li_{0.53}Na_{0.47})_2CO_3$ melt at 923 K under $P_{O_2} : P_{CO_2} = 0.9 : 0.1$ atm. (○): Au, (●): NiO, (■): $NiCO_3$.

consistent with the fact that there is no peak attributed to $NiCO_3$ in XRD (Fig. 3) of sample no. 6, which was withdrawn after 6 h of immersion.

Change in lattice parameter of NiO and lithium content derived by Eq. (2) in immersion time is shown in Fig. 11. The sample withdrawn at 12 h of immersion exhibited larger standard deviation than the others because of the hindrance of impurities (see Fig. 9). Increase of lithium content before 72 h is slight or insignificant because of relatively large standard deviations. Lithium content reached 0.033(3) after 200 h of immersion, which is smaller than in the case of Li/K eutectic. However, the lattice parameter (lithium content) is a decreasing (increasing) trend even at 200 h. Thus, the intrinsic value of lithium content in NiO oxidized in Li/Na melt is still unclear in this work. Belhomme et al. [19] reported that Li content in ex situ synthesized $Li_xNi_{1-x}O$ ($0 < x < 0.5$) compounds reaches a value relatively close to 0.05 after 48 h of immersion in Li/Na melt. From our results, however, a Li content larger than 0.033 can be expected, and slower lithiation of NiO in Li/Na eutectic than in Li/K melt.

3.3. Difference in OCP curve between Li/K and Li/Na

A mixed potential concept can elucidate the fact that the potential arrest at Ni(II)/Ni(III) system in Li/Na (Stage I in Fig. 6) is much shorter in time than in Li/K (Stage II

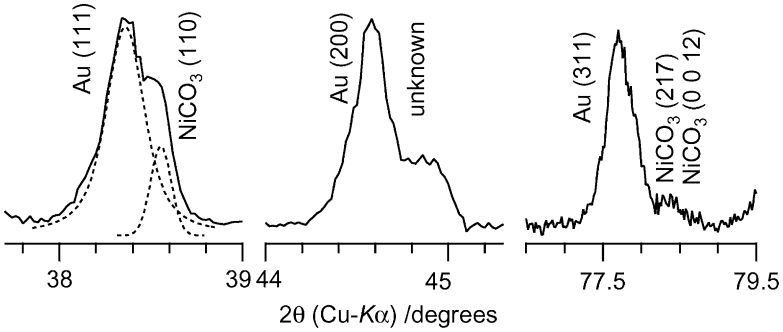

Fig. 9. Magnified view of Fig. 6. Reflection of Cu $K\alpha_2$ was subtracted to distinguish overlapped peaks.

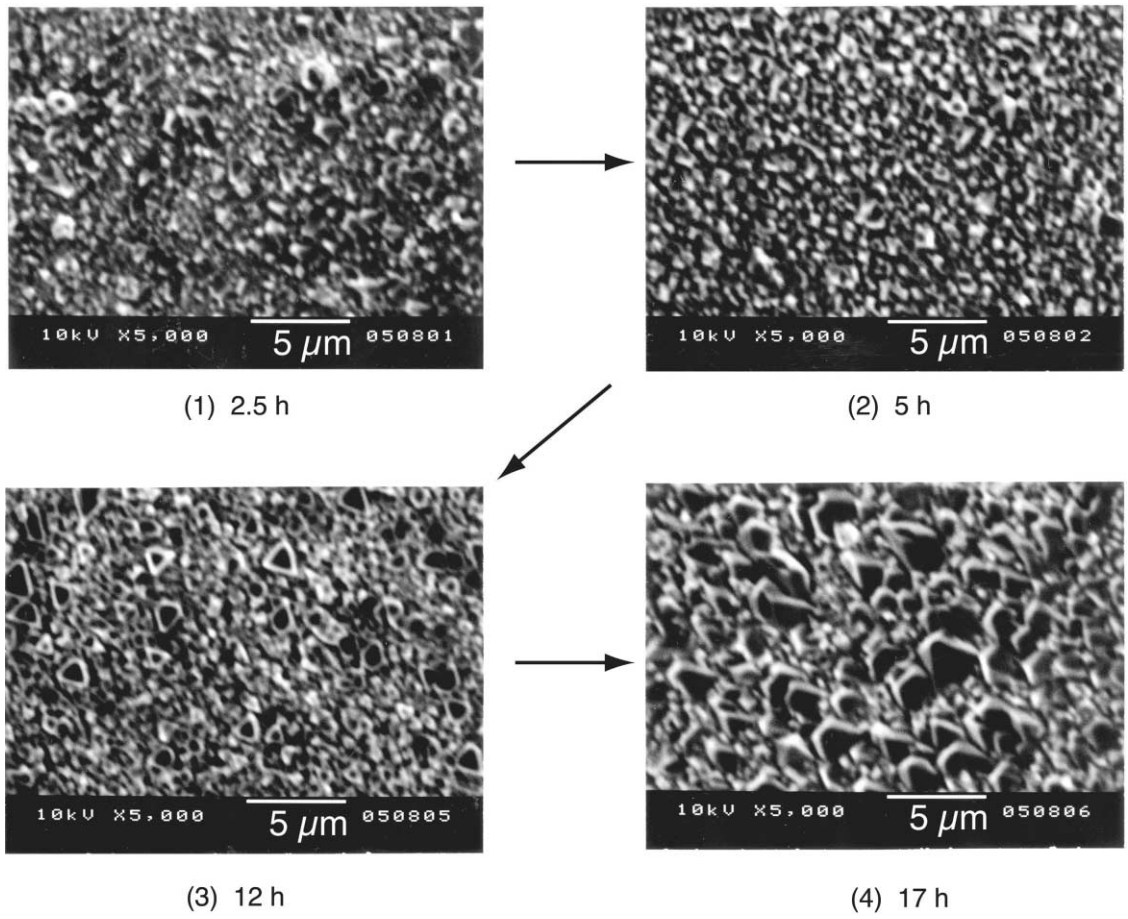

Fig. 10. Scanning microscopic images (1–4) of Ni/Au samples withdrawn at various time of exposure from $(Li_{0.53}Na_{0.47})_2CO_3$ melt at 923 K under $P_{O_2} : P_{CO_2} = 0.9 : 0.1$ atm.

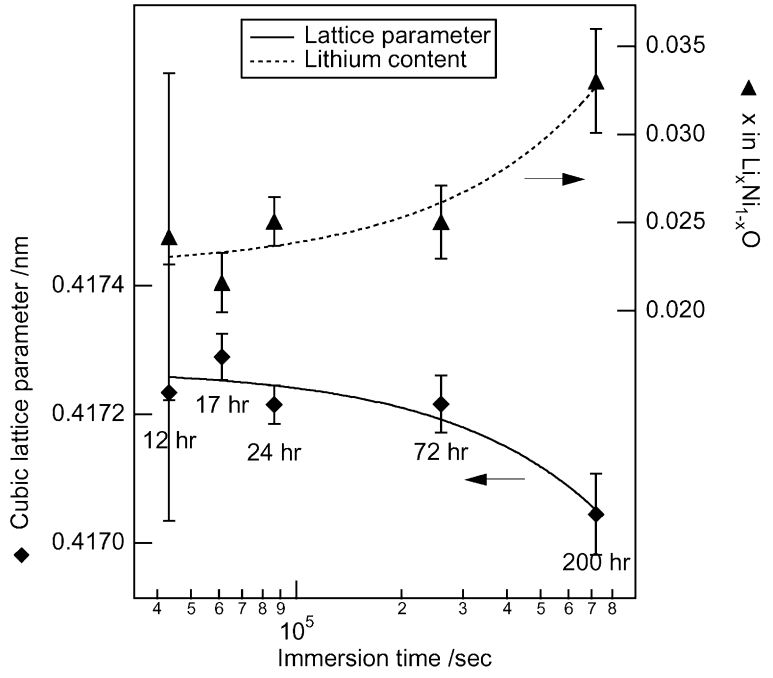

Fig. 11. Change in cubic lattice parameter and Li content of pre-oxidized NiO with time in $(Li_{0.53}Na_{0.47})_2CO_3$ melt at 923 K under $P_{O_2} : P_{CO_2} = 0.9 : 0.1$ atm.

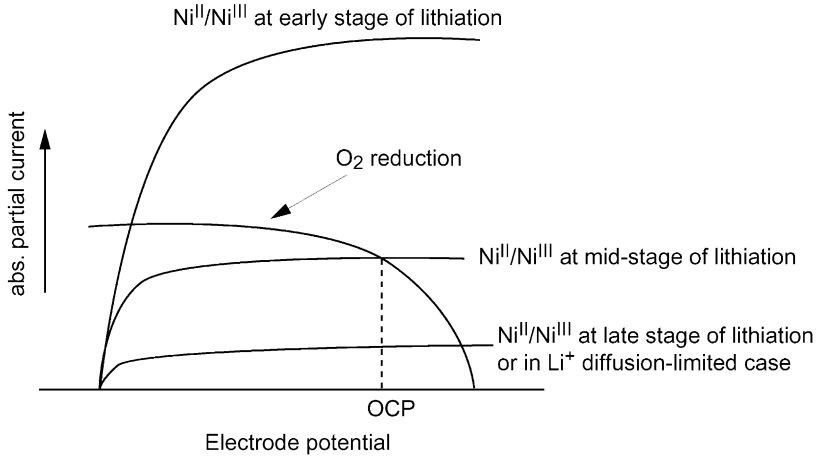

Fig. 12. Schematic drawing of mixed potential formation for Ni oxidation and O_2 reduction at Ni/Au electrode.

in Fig. 2). Fig. 12 shows a schematic drawing of the OCP formation at a Ni/Au during in situ lithiation. Oxygen reduction is postulated as a counterpart reaction for the oxidation of Ni(II) to Ni(III). The potential arrests of Stage II in Li/K, and Stage I in Li/Na occur when O_2 reduction is the diffusion-limited reaction on the mixed potential of Ni/Au. In the case of Li/Na, the potential arrest around −0.5 V versus SOE (Stage I in Fig. 6) would evolve during a short period of time when only the surface layer of NiO is lithiated. Then the reaction site of lithiation shifts toward the inside of NiO film, and diffusion of Li^+ into NiO will be obstructed by the dense NiO bulk. Thus, the Li^+ diffusion into NiO lattice becomes the limiting reaction instead of O_2 diffusion on the mixed potential on the Ni/Au. This results in an anodic shift of OCP (Stage II in Li/Na) even before completion of lithiation. On the other hand, faster diffusion of Li^+ into NiO in Li/K can be postulated based on the series of lattice parameter mentioned earlier. Consequently, it is believed that partial current of Ni(II) to Ni(III) oxidation accompanied by lithiation is higher in Li/K than in Li/Na. This justifies the potential arrest of Ni(II)/Ni(III) system in Li/K being longer in time than in Li/Na.

4. Conclusion

The change in Li content of in situ formed $Li_xNi_{1-x}O$ with time has been estimated by XRD method. Lithium content, x, of the sample immersed in molten carbonate reached 0.041 and 0.033 in Li/K and Li/Na melt, respectively after 200 h of immersion. Change in Li content with time revealed two conspicuous features on the in situ lithiation (i) the lithiation reaction continues even after the electrode potential of NiO reached the oxygen reduction equilibrium potential, and (ii) lithiation reaction is faster in Li/K melt than in Li/Na. The XRD measurements coupled with SEM also revealed that the decomposition of an unstable intermediate, namely $NiCO_3$, during in situ NiO formation in Li/Na melt results in drastic change of surface morphology.

Acknowledgements

This work was partly supported by the Proposal-Based Immediate-Effect R&D Promotion Program no. 98Z31-011 from the New Energy and Industrial Technology Development Organization (NEDO).

References

[1] B.S. Baker, J. Power Sources 86 (2000) 9.
[2] T. Ishikawa, H. Yasue, J. Power Sources 86 (2000) 145.
[3] T. Fukui, H. Okawa, T. Tsunooka, J. Power Sources 71 (1998) 239.
[4] I. Uchida, Y. Mugikura, T. Nishina, K. Itaya, J. Electroanal. Chem. 206 (1986) 241.
[5] T. Nishina, K. Takizawa, I. Uchida, J. Electroanal. Chem. 263 (1989) 87.
[6] K. Yamada, I. Uchida, Chem. Lett. (1994) 299.
[7] K. Yamada, I. Uchida, J. Electroanal. Chem. 385 (1995) 57.
[8] P. Tomczyk, H. Sato, K. Yamada, T. Nishina, I. Uchida, J. Electroanal. Chem. 391 (1995) 133.
[9] C.G. Lee, K. Yamada, T. Nishina, I. Uchida, J. Power Sources 62 (1996) 145.
[10] K. Yamada, N. Sato, T. Fujino, M. Nishizawa, I. Uchida, Electrochemistry 67 (1999) 68.
[11] M. Mohamedi, Y. Hisamitsu, K. Kihara, T. Kudo, T. Itoh, I. Uchida, J. Alloys Comp. 315 (2001) 224.
[12] T. Kudo, Y. Hisamitsu, K. Kihara, M. Mohamedi, I. Uchida, J. Appl. Electrochem., in press.
[13] T. Nishina, K. Takizawa, I. Uchida, J. Electroanal. Chem. 263 (1989) 87.
[14] P. Tomczyk, H. Sato, K. Yamada, T. Nishina, I. Uchida, J. Electroanal. Chem. 391 (1995) 125.
[15] M.S. Yazici, J.R. Selman, Solid State Ionics 124 (1999) 149.
[16] M. Mohamedi, Y. Hisamitsu, T. Kudo, T. Itoh, I. Uchida, J. Solid State Electrochem. 5 (2001) 538.
[17] K. Hotoh, J. Niikura, E. Yasumoto, T. Gamo, Denki Kagaku (Electrochemistry) 64 (1996) 825.
[18] C. Belhomme, M. Cassir, C. Tessier, E. Berthoumieux, Electrochem. Solid State Lett. 3 (2000) 216.
[19] C. Belhomme, M. Cassir, J. Devynck, G. Gregoire, J. Mater. Sci. 35 (2000) 2683.
[20] I. Uchida, T. Nishina, Y. Mugikura, K. Itaya, J. Electroanal. Chem. 206 (1986) 229.

[21] I. Uchida, T. Nishina, Y. Mugikura, K. Itaya, J. Electroanal. Chem. 206 (1986) 241.
[22] I. Uchida, T. Nishina, Y. Mugikura, K. Itaya, J. Electroanal. Chem. 209 (1986) 125.
[23] T. Sato, C. Hsin-Chang, T. Endo, M. Shimada, J. Mater. Sci. Lett. 5 (1986) 552.
[24] W. Li, J.N. Reimers, J.R. Dahn, Phys. Rev. B 46 (1992) 3236.
[25] J.R. Selman, H.C. Maru, in: G. Mamantov, J. Braunstein (Eds.), Advances in Molten Salt Chemistry, Vol. 4, Plenum Press, New York, 1983, p. 323.
[26] B.K. Andersen, Thermodynamic Properties of Molten Alkali Carbonates, Doctorial Thesis, Technical University of Denmark, Lyngby, Denmark, 1975.
[27] P. Tomczyk, M. Mosialek, J. Electroanal. Chem. 463 (1999) 72.